



Neutron diffraction study on hydrostatic pressure regulated magnetostructural transition and magnetocaloric effect in $\text{MnNi}_{1-x}\text{Fe}_x\text{Si}_{1-y}\text{Ge}_y$ alloys

Cite as: J. Appl. Phys. **127**, 133905 (2020); <https://doi.org/10.1063/5.0003056>

Submitted: 30 January 2020 . Accepted: 20 March 2020 . Published Online: 06 April 2020

Fei-Ran Shen,  Feng-Xia Hu, Zi-Bing Yu, Hou-Bo Zhou, Hui Wu, Qing-Zhen Huang, Jia-Zheng Hao, Yi-Hong Gao, Kai-Ming Qiao, Jia Li, Cheng Zhang, Wen-Hui Liang, Lun-Hua He,  Jing Wang, Tian-Jiao Liang, Ji-Rong Sun, and Bao-Gen Shen

COLLECTIONS

Paper published as part of the special topic on [Multicalorics MUCA2020](#)



View Online



Export Citation



CrossMark

ARTICLES YOU MAY BE INTERESTED IN

[Temperature and pH responsive behavior of antifouling zwitterionic mesoporous silica nanoparticles](#)

Journal of Applied Physics **127**, 135106 (2020); <https://doi.org/10.1063/1.5140707>

[In situ polymerization and polymer grafting to stabilize polymer-functionalized nanoparticles in polymer matrices](#)

Journal of Applied Physics **127**, 134701 (2020); <https://doi.org/10.1063/1.5144212>

[Erratum: "Resolving the ultrafast intersystem crossing in a bimetallic platinum complex" \[J. Chem. Phys. **151**, 114303 \(2019\)\]](#)

The Journal of Chemical Physics **152**, 169902 (2020); <https://doi.org/10.1063/5.0009294>



Your Qubits. Measured.

Meet the next generation of quantum analyzers

- Readout for up to 64 qubits
- Operation at up to 8.5 GHz, mixer-calibration-free
- Signal optimization with minimal latency

Find out more



Neutron diffraction study on hydrostatic pressure regulated magnetostructural transition and magnetocaloric effect in $\text{MnNi}_{1-x}\text{Fe}_x\text{Si}_{1-y}\text{Ge}_y$ alloys

Cite as: J. Appl. Phys. 127, 133905 (2020); doi: 10.1063/5.0003056

Submitted: 30 January 2020 · Accepted: 20 March 2020 ·

Published Online: 6 April 2020



Fei-Ran Shen,^{1,2,3} Feng-Xia Hu,^{1,2,4,a)} Zi-Bing Yu,^{1,2} Hou-Bo Zhou,^{1,2} Hui Wu,⁵ Qing-Zhen Huang,⁵ Jia-Zheng Hao,¹ Yi-Hong Gao,^{1,2} Kai-Ming Qiao,^{1,2} Jia Li,^{1,2} Cheng Zhang,^{1,2} Wen-Hui Liang,^{1,2} Lun-Hua He,^{1,3,5,a)} Jing Wang,^{1,2,6} Tian-Jiao Liang,³ Ji-Rong Sun,^{1,2,4} and Bao-Gen Shen^{1,2,4}

AFFILIATIONS

¹Beijing National Laboratory for Condensed Matter Physics and State Key Laboratory of Magnetism, Institute of Physics, Chinese Academy of Sciences, Beijing 100190, People's Republic of China

²School of Physical Sciences, University of Chinese Academy of Sciences, Beijing 100049, People's Republic of China

³Spallation Neutron Source Science Center, Dongguan 523803, China

⁴Songshan Lake Materials Laboratory, Dongguan, Guangdong 523808, People's Republic of China

⁵NIST Center for Neutron Research, National Institute of Standards and Technology, Gaithersburg, Maryland 20899, USA

⁶Fujian Innovation Academy, Chinese Academy of Sciences, Fuzhou, Fujian 350108, People's Republic of China

Note: This paper is part of the Special Topic on Multicalorics.

a) Authors to whom correspondence should be addressed: fxhu@iphy.ac.cn and lhhe@iphy.ac.cn

ABSTRACT

Ni_2In -type hexagonal compounds $\text{MM}'\text{X}$ (M, M' = transition metals, X = main element) involving magnetostructural transition (MST) have attracted much attention due to their giant magnetocaloric effect (MCE). Physical pressure, as an effective method, has been used to adjust the MST and the resultant MCE. Enhanced and diminished MCEs by hydrostatic pressure were both reported previously, but the underlying mechanism is unclear. Here, we report our neutron diffraction study on MST and MCE regulated by hydrostatic pressure in $\text{MnNi}_{1-x}\text{Fe}_x\text{Si}_{1-y}\text{Ge}_y$ alloys. Careful refinements indicate that the martensitic phase shows a linear ferromagnetic structure with spin moment confined on Mn sites, which remains almost unchanged at pressures lower than 5 kbar even though slight compressions of Mn–Mn bond lengths can be identified. The MST keeps sharp under pressures lower than 5 kbar, while the derived volume change ($\Delta V/V$) across MST reduces 7%, i.e., from 2.84% (0 kbar) to 2.63% (2.1 kbar), due to the effect of pressure on two-phase coexistence. Accordingly, the estimated lattice entropy change (ΔS_{Latt}) based on the Debye approximation reduces by 10% from 37.1 J/kg K (0 kbar) to 33.5 J/kg K (2.1 kbar). These ΔS_{Latt} values, driven by temperature, are all somewhat larger than the magnetic entropy change driven by a 5 T magnetic field. This result may imply that a magnetic field of 5 T is not sufficient for the MST to complete. As the pressure reaches 5 kbar, the MST notably slows down. This may originate from the extended temperature region of two-phase coexistence but not the decoupling of MST.

Published under license by AIP Publishing. <https://doi.org/10.1063/5.0003056>

I. INTRODUCTION

Solid magnetic refrigeration based on the magnetocaloric effect (MCE) has been considered as an alternative to conventional vapor-compression refrigeration techniques owing to the advantages of energy conservation and environmental friendliness.^{1,2} For the materials with giant MCE, the magnetic phase transition is usually accompanied by discontinuous changes in lattice parameters or crystal symmetry,

such as $\text{Gd}_5(\text{Si,Ge})_4$,³ $\text{MnFeP}_{1-x}\text{As}_x$,⁴ MnAs ,^{5,6} $\text{La}(\text{Fe,Si})_{13}$,^{7–9} and NiMn -based Heusler alloys.^{10–12} Therefore, hydrostatic pressure is an effective means to tune the magnetostructural/magnetoelastic transition and the consequent MCE by modifying atomic environments and exchange coupling.

Ni_2In -type hexagonal compounds $\text{MM}'\text{X}$ (M, M' = transition metals, X = main element) have recently attracted renewed attention

due to their large magnetocaloric MCE,¹³ barocaloric effect (BCE),¹⁴ and giant negative thermal expansion (NTE) behavior^{15,16} involving the magnetostructural transition (MST). As a member of the MM'X family, the MnNiSi alloy undergoes martensitic structural transition T_S from Ni₂In-type hexagonal to TiNiSi-type orthorhombic phase at $T_S \sim 1206$ K, and the martensite shows the ferromagnetic (FM) ground state with a Curie temperature at $T_C \sim 620$ K.¹⁷ The large temperature gap between these two transitions makes it hard to realize the magnetostructure coupling. Fortunately, another family member MnFeGe with a hexagonal structure shows a reasonably low $T_C \sim 159$ K. Through isostructurally alloying MnNiSi with MnFeGe, both T_C and T_S of MnNiSi can be reduced. During this process, the Si atoms are replaced by the Ge, which has the same number of covalent electrons but a larger atom radius. Thus, the Mn–Mn interatomic distances are enlarged, which changes the magnetic interactions between Mn–Mn atoms and favors the antiferromagnetic (AFM) coupling.^{18–20} As a result, the FM order gradually transforms into AFM order, and the magnetic transition temperature decreases. Meanwhile, the Ni atoms are substituted by the Fe, which has nearly the same atomic radius but different number of covalent electrons. The introduction of Fe atoms can promote FM coupling.¹³ Besides, the Fe–Ge(Si) layers have a stronger covalent bonding than Ni–Ge(Si) layers,¹³ which would help stabilize the hexagonal structure and shift the T_S to a low temperature. Eventually, coupled MST from paramagnetic (PM) austenite to FM martensite can be realized.

Recently, Samanta *et al.* reported the pressure enhanced MCE in MnNiSi-based alloys with MST, which was considered to be from pressure enhanced lattice entropy change (ΔS_{Latt}). According to the relation between the ΔS_{Latt} and the volume change $\Delta V/V$ across the transition, i.e., $\delta[\Delta V/V (\%)]/\delta(\Delta S_{\text{st}}) = 0.08(\text{J/kg K})^{-1}$, the enhanced $\Delta V/V$ as high as 7% by pressure was evaluated.²¹ However, the enhancement of MCE driven by pressure was not observed in a similar hexagonal alloy Mn_{0.93}Co_{0.07}CrGe.²² At low pressures, Caron *et al.* found that the magnitude of entropy change stays nearly unchanged. When the pressure reaches a critical value, the phase transition slows down, accompanied by a significant decrease of MCE. The decoupling of MST was proposed to be the origin, but the related mechanism is still unclear. The evolution of the local atomic environments and magnetic structure under pressure has not been reported.

In this paper, we prepared MnNi_{1-x}Fe_xSi_{1-y}Ge_y alloys. It was found that both Fe- and Ge-doping can effectively lower the martensitic transition temperature. MST was discerned in several alloy compositions. The evolution of MST and MCE under pressure was studied by high-resolution neutron powder diffraction (NPD) with *in situ* pressure applied. Detailed refinements revealed that the martensitic orthorhombic phase shows a linear FM structure with magnetic moment confined on Mn sites, and no obvious moment was found at Fe sites. Moreover, the refined magnetic moment on Mn sites does not show obvious change even though slight compressions of Mn–Mn bond lengths can be identified under pressure. The MST keeps sharp under pressures lower than 5 kbar but notably slows down as the pressure reaches 5 kbar, which originates from the extended two-phase coexistent temperature region, instead of the decoupling of MST. Moreover, the derived volume change ($\Delta V/V$) across MST does not show any enhancements but

reduces 7% as a pressure of 2.1 kbar is applied. Accordingly, the lattice entropy change (ΔS_{Latt}) reduces by 10%, which is estimated based on the Debye approximation. However, these ΔS_{Latt} values driven by temperature are all somewhat larger than the magnetic entropy change (ΔS_{Mag}) driven by a 5 T magnetic field, implying that a magnetic field of 5 T may not be adequate to prompt an MST completed.

II. EXPERIMENTAL DETAILS

MnNi_{1-x}Fe_xSi_{1-y}Ge_y ($0.53 \leq x \leq 0.56$, $0.44 \leq y \leq 0.64$) compounds were prepared by arc-melting appropriate amounts of starting materials with purities of >99% in a high-purity argon atmosphere (99.996%) with a base pressure of 10^{-4} Pa. In order to compensate the weight loss during the melting, 3 wt. % excessive Mn was added. The alloy was turned over and remelted for three times during the arc-melting process to ensure homogeneity. The obtained ingots were wrapped separately with Mo foil and subsequently homogenized in a sealed quartz tube under a high vacuum at 1023 K for 3 days and then followed by quenching in liquid nitrogen. High-resolution NPD under different hydrostatic pressures was performed at the NIST Center for Neutron Research (NCNR) on the BT-1 high-resolution neutron powder diffractometer. A Ge (311) monochromator was used to produce a monochromatic neutron beam of wavelength 2.0775 Å. The crystal and magnetic structures were refined by the Rietveld method using the General Structure Analysis System (GSAS) suite of programs. Magnetic measurements under hydrostatic pressure were performed using a superconducting quantum interference device magnetometer (MPMS-7T) in a BeCu cylindrical pressure cell. Daphne 7373 oil was used as the pressure transmitting medium. The pressure was calibrated by measuring the shift of a superconducting transition temperature of Pb placed together with samples.

III. RESULTS AND DISCUSSION

Temperature dependent magnetization (M–T curves) were measured under 0.1 T for MnNi_{1-x}Fe_xSi_{1-y}Ge_y ($0.53 \leq x \leq 0.56$, $0.44 \leq y \leq 0.64$) alloys, as shown in Fig. 1. The Fe- and Ge-doping can both effectively drive the martensitic transition to lower temperature, as the Fe doping helps enhance the covalent strength in the Fe(Ni)–Ge(Si) layer, while the Ge-doping changes the chemical pressure in the compounds.¹⁸ As a result, coupled MST can be realized in three components ($x = 0.54$, $y = 0.54$; $x = 0.55$, $y = 0.54$; $x = 0.53$, $y = 0.54$), characterized by sharp magnetic transitions from FM to PM state with thermal hysteresis. The components ($x = 0.56$, $y = 0.54$; 0.54 , $y = 0.64$) undergo pure magnetic transition with second-order in nature. The peaks appeared around 170 K might be relative to the strong competition between AFM and FM interactions, and the exact origin requires further studies.

To investigate the evolution of the crystal structure and the magnetic structure under pressure, MnNi_{1-x}Fe_xSi_{1-y}Ge_y ($x = 0.53$, $y = 0.54$) with MST was chosen and studied by NPD with *in situ* pressure applied simply considering its higher MST temperature compared to the other two ($x = 0.54$, $y = 0.54$; $x = 0.55$, $y = 0.54$). The component with higher MST facilitates big pressure applied noting that the pressure drives the MST to lower temperature. Figures 2(a) and 2(b) show the representative refined NPD patterns

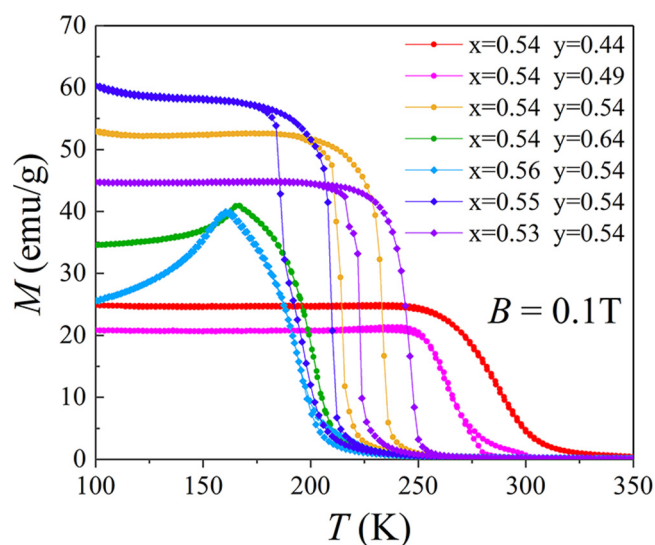


FIG. 1. Temperature dependence of magnetization (M - T curves) upon heating and cooling under 0.1 T for $\text{MnNi}_{1-x}\text{Fe}_x\text{Si}_{1-y}\text{Ge}_y$ ($0.53 \leq x \leq 0.56$, $0.44 \leq y \leq 0.64$) alloys.

at 175 K/0 kbar and 130 K/5 kbar, respectively. Careful refinements indicate that the martensitic orthorhombic phase possesses a linear FM structure with the magnetic moments confined on Mn sites and the direction along the b axis [Fig. 2(c)]. No obvious magnetic moment is found at Fe sites. We also refined the possibility of the Mn sites occupied by Fe. Note that the nuclear scattering lengths of Mn and Fe are very different. If the Fe partially occupies the Mn sites, it can be easily resolved from the NPD data. We tried to add Fe atoms to the Mn site during the modeling process for the NPD data collected at 175 K/0 kbar. The initial occupation of Fe and Mn atoms is set to 50%, and the sum is limited to 1 during the refining process. The refinement result indicates that the occupation of Mn atoms is 99.2(5)% and the occupation of Fe atoms is 0.8(5)%, which indicates that the Mn sites should be occupied by Mn rather than Fe atoms.

At 175 K under 0 kbar, the refined moment is $2.68(10) \mu_B$ on Mn atom, which appears to be $2.67(10) \mu_B$ and $2.67(10) \mu_B$ under 1 kbar and 2 kbar, respectively (Table I). As the pressure increases to 5 kbar, the phase fraction of the orthorhombic phase remarkably declines, making it difficult to accurately determine the magnetic moments. Reducing the temperature to 130 K under 5 kbar, the orthorhombic phase fraction can be raised to 81%, and the refined moment on Mn atom is $2.71(10) \mu_B$. All these refined moments approximately match the corresponding magnetization values in the M - T curves measured at a 5 T magnetic field (Fig. 3) with the corresponding ratio of orthorhombic and hexagonal phases taken into account (see details in the following). Moreover, it can be seen that the moment on Mn sites remains almost unchanged within the error range regardless of pressure (Table I). During refinements, no magnetic moment is detected for the austenitic hexagonal phase at 130 K or higher temperatures, indicating that the austenitic hexagonal phase remains as PM.

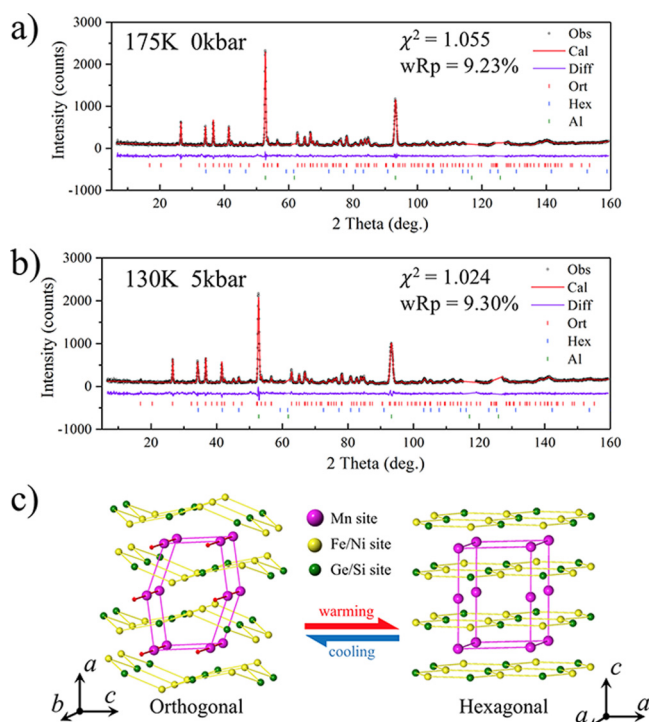


FIG. 2. Observed (black circle), calculated (red line) neutron diffraction patterns, their difference (purple line), orthorhombic phase peak positions (red bar), hexagonal phase peak positions (blue bar), Al (sample holder) peak positions (green bar) for $\text{MnNi}_{0.47}\text{Fe}_{0.53}\text{Si}_{0.46}\text{Ge}_{0.54}$ collected at (a) $T = 200$ K, $P = 0$ kbar and (b) $T = 130$ K, $P = 5$ kbar by BT-1. (c) Sketches of the ferromagnetic orthorhombic structure and the paramagnetic hexagonal structure for $\text{MnNi}_{0.47}\text{Fe}_{0.53}\text{Si}_{0.46}\text{Ge}_{0.54}$.

Figure 3 shows the M - T curves of $\text{MnNi}_{0.47}\text{Fe}_{0.53}\text{Si}_{0.46}\text{Ge}_{0.54}$ upon heating and cooling measured at a 5 T magnetic field under different pressures. It can be found that the pressure can drive the martensitic transition to lower temperatures at a rate of $dT_M/dP \approx -15$ K/kbar. This is because the pressure stabilizes the hexagonal phase with a smaller cell volume. When the pressure is less than 5 kbar, the phase transition remains steep, while the magnetization of the martensitic orthorhombic phase shows a slight reduction with increasing pressure at a given temperature. For example, at 175 K, the derived average magnetic moment on Mn atoms reduces from $2.56 \mu_B/\text{Mn}$ to $2.39 \mu_B/\text{Mn}$ as the pressure increases from 0 to 2.1 kbar and sharply drops to $1.79 \mu_B$ at 5 kbar (Table I). The deviations of these values from the NPD refined results might be due to the coexistence of the non-magnetic hexagonal phase (see details in following discussion). On the other hand, the MST also behaves sensitive to the magnetic field. The comparison of the normalized M - T curves measured between 0.1 T and 5 T fields under atmospheric pressure is shown in the inset of Fig. 3. It can be found that the external magnetic field can drive the MST to high temperatures. The MST locates around ~ 257 K at 5 T, which is 12 K higher than the MST ~ 245 K at 0.1 T. The equivalent driving rate dT_M/dH is about $+2.4$ K/T.

TABLE I. Lattice and magnetic information derived from NPD, including lattice parameters, volume, the fraction of the orthorhombic phase, the parameters x and z of Mn site, Mn–Mn bond lengths, and refined magnetic moment M_{Mn} for the martensitic orthorhombic phase of $\text{MnNi}_{0.47}\text{Fe}_{0.53}\text{Si}_{0.46}\text{Ge}_{0.54}$. The average molecular magnetic moment on Mn atoms $M_{\text{Mn}}/\text{f.u.}$ derived from M–T curves under a 5 T magnetic field is also given for comparison.

	175 K				130 K
	0 kbar	1 kbar	2 kbar	5 kbar	5 kbar
a-axis length (Å)	5.8709(4)	5.8664(3)	5.8615(3)	5.8525(6)	5.8449(4)
b-axis length (Å)	3.7344(3)	3.7333(2)	3.7330(3)	3.7289(5)	3.7238(3)
c-axis length (Å)	7.0723(5)	7.0686(4)	7.0656(4)	7.0543(8)	7.0623(5)
Volume (Å ³)	155.06(2)	154.81(2)	154.60(2)	153.95(4)	153.71(2)
Fraction of Orth. (%)	95.0(8)	91.2(8)	87.3(8)	40.9(8)	80.9(8)
Mn site	x	x	x	x	x
	0.0300(13)	0.0305(13)	0.0312(14)	0.0331(21)	0.0341(15)
	z	z	z	z	z
	0.6827(11)	0.6825(11)	0.6825(11)	0.6819(17)	0.6816(12)
Mn–Mn (d_1) (Å)	3.086(5)	3.084(5)	3.081(5)	3.080(8)	3.078(5)
Mn–Mn (d_2) (Å)	3.208(13)	3.205(13)	3.208(13)	3.196(21)	3.195(14)
M_{Mn} from NPD (μ_{B})	2.68(10)	2.67(10)	2.67(10)	...	2.71(10)
$M_{\text{Mn}}/\text{f.u.}$ from M–T curves (μ_{B})	0 kbar	1.3 kbar	2.1 kbar	5.0 kbar	5 kbar
	2.56	2.47	2.39	1.79	2.20

To know more details of atomic environments under pressure, the refined lattice information including the Mn–Mn bond lengths of the orthorhombic phase under different pressures are summarized in Table I and Fig. 4. All unit cell parameters a , b , c , as well as the volume, show slight compression under pressure. As a response, the Mn–Mn (d_1) and Mn–Mn (d_2) lengths [Figs. 4(b) and 4(c)] also reduce but remain within a small range, i.e., $3.080 \text{ \AA} \leq d_1 \leq 3.086 \text{ \AA}$, $3.196 \text{ \AA} \leq d_2 \leq 3.208 \text{ \AA}$. For such Mn-based

TiNiSi-type martensite, the magnetic structure is a result from the competition between direct exchange of Mn–Mn (d_1) and superexchange of Mn–Mn (d_2), while the former plays a dominant role. Density functional theory (DFT) calculations^{19,20} revealed that the magnetic ground state critically depends on the d_1 length. For $d_1 \leq 2.5 \text{ \AA}$, the close distance between Mn atoms leads to a strong overlap of their 3d orbitals, and no magnetic ground state is stable due to the broad 3d hybrid bands. As the d_1 length increases, the overlap of the 3d orbitals of Mn becomes smaller, resulting in more localized 3d electrons and enhanced exchanges between Mn atoms. For $2.5 \text{ \AA} \leq d_1 \leq 2.9 \text{ \AA}$, the FM ground state shows lower energy compared to AFM, while for $2.9 \text{ \AA} \leq d_1 \leq 3.3 \text{ \AA}$, the AFM state shows lower energy than the FM state. With further increasing d_1 length to $d_1 \geq 3.3 \text{ \AA}$, the FM state prevails again. For the present $\text{MnNi}_{0.47}\text{Fe}_{0.53}\text{Si}_{0.46}\text{Ge}_{0.54}$ alloy, d_1 appears in the range of $3.080 \text{ \AA} \leq d_1 \leq 3.086 \text{ \AA}$ with varying pressures, which should favor AFM coupling.^{19,20} However, the Fe doping can introduce a new FM coupling between Mn atoms,¹³ which makes the FM order more stable. As a result, the $\text{MnNi}_{0.47}\text{Fe}_{0.53}\text{Si}_{0.46}\text{Ge}_{0.54}$ alloy exhibits a linear FM structure. Although the application of pressure can somewhat compress the Mn–Mn bond lengths, the altered magnitude is not enough to obviously affect the exchange interaction. This might be the reason why we did not detect obvious change of the magnetic structure and the magnetic moment with pressure from the NPD refinements (Table I).

Moreover, the refined results from NPD patterns indicate that the application of pressure largely extends the coexistent temperature region of the FM orthorhombic and the non-magnetic hexagonal phases and slows down the MST, particularly for the case of 5 kbar. Figure 5(a) shows the refined ratio of the orthorhombic and hexagonal phases as a function of temperature under different pressures. With increasing pressure, the martensitic transformation clearly moves to low temperature. This also means that the pressure drives the transition from orthorhombic to hexagonal phase. For example, at 175 K, the orthorhombic ratio gradually reduces with

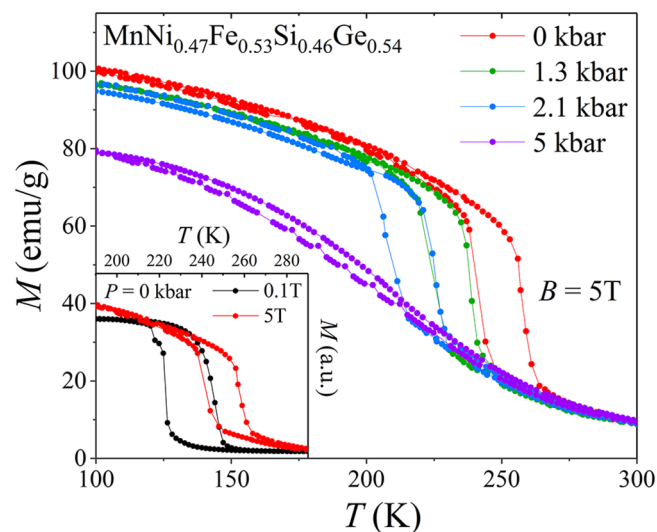


FIG. 3. Temperature dependence of magnetization (M–T curve) measured upon heating and cooling at a 5 T magnetic field with various pressures for $\text{MnNi}_{0.47}\text{Fe}_{0.53}\text{Si}_{0.46}\text{Ge}_{0.54}$. The inset shows the normalized magnetization as a function of temperature for 0.1 T and 5 T magnetic fields under atmospheric pressure.

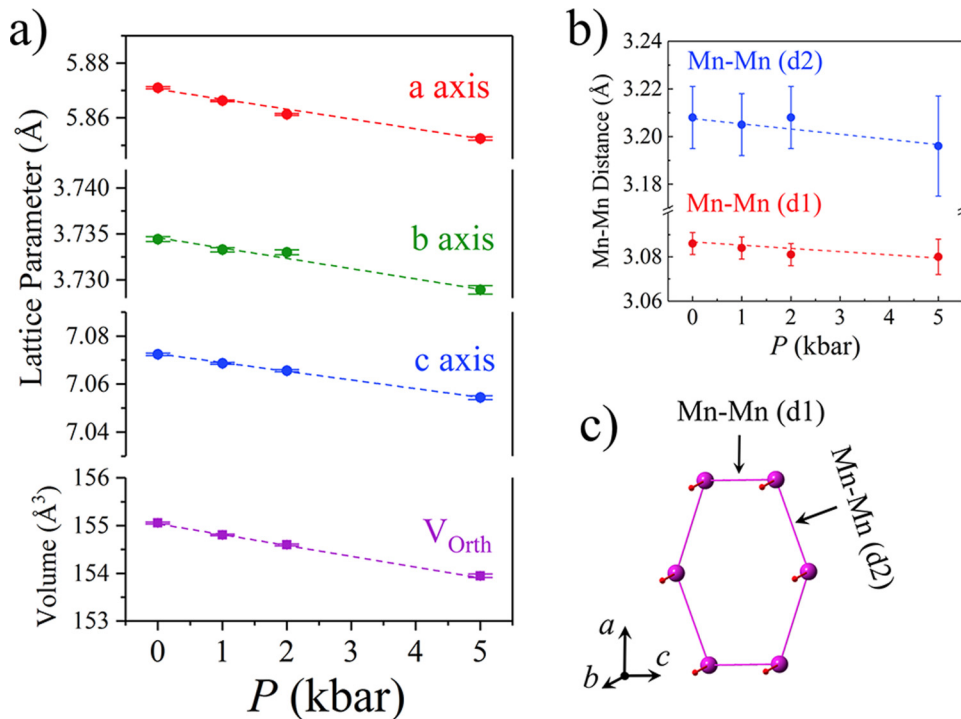


FIG. 4. (a) The refined lattice parameters, volume of the orthorhombic phase as a function of pressure at a given temperature 175 K, and (b) the corresponding Mn-Mn (d₁) and Mn-Mn (d₂) distance as a function of pressure for $\text{MnNi}_{0.47}\text{Fe}_{0.53}\text{Si}_{0.46}\text{Ge}_{0.54}$, where the relevant error bars have been given. (c) Sketch of the FM structure of the orthorhombic phase with labeled d₁ and d₂ bonds.

pressure, e.g., 95.0(8)%, 91.2(8)%, 87.3(8)%, and 40.9(8)%, at 0 kbar, 1 kbar, 2 kbar, and 5 kbar, respectively. We evaluated the steepness of the MST by measuring the breadth of the temperature range with varying pressures to convert the same fraction of the orthorhombic phase to the hexagonal phase. For example, under 0 kbar, the orthorhombic phase ratio increases from 5% to 80% within a temperature window of 25 K (262K–237 K), while under the pressures of 1 kbar, 2 kbar, and 5 kbar, for the same amount of the phase fraction change, the required temperature windows are 28 K (248K–220 K), 42 K (200K–242 K), and 62 K (192 K–130 K), respectively. It can be found that the MST becomes slightly less sharp under a small pressure. When the pressure reaches 5 kbar, the MST broadens significantly, which is accompanied by the

remarkably extended temperature region of the coexistent FM orthorhombic and the non-magnetic hexagonal phases, instead of decoupling of MST. This also explains why the derived magnetic moments on average Mn atoms from the M–T curves (Fig. 3) are all smaller than the NPD refined results on the single FM orthorhombic phase (Table I).

Based on the refined phase fraction and the corresponding lattice parameters, the calculated average cell volumes, V , as a function of temperature under different pressures are shown in the inset of Fig. 5(b). As the pressure increases from 0 kbar to 2 kbar, the maximal $\Delta V/V$ across the MST reduces from 2.84% to 2.63%, as shown in Fig. 5(b). This indicates that the temperature driven lattice entropy change, ΔS_{Latt} , during the MST will decrease with

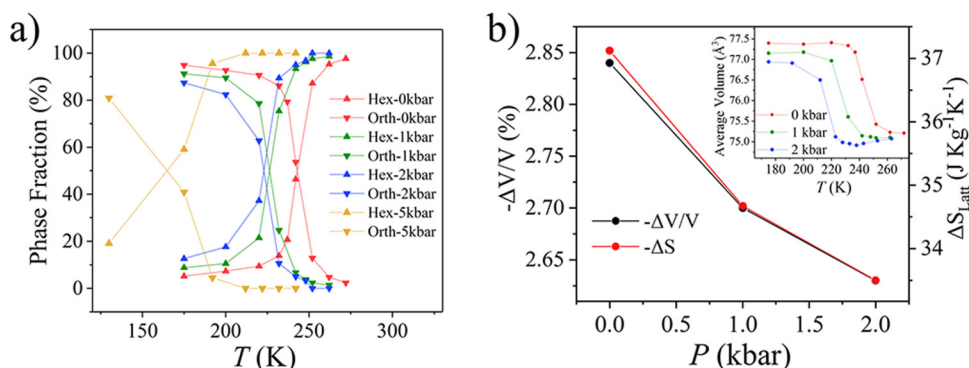


FIG. 5. (a) Temperature dependence of orthorhombic (Orth.) and hexagonal (Hex.) phase fractions under different hydrostatic pressures for $\text{MnNi}_{0.47}\text{Fe}_{0.53}\text{Si}_{0.46}\text{Ge}_{0.54}$. (b) The derived average cell volume changes $\Delta V/V$, and the corresponding lattice entropy changes ΔS_{Latt} across the MST, under different hydrostatic pressures. The lines guide eyes. The inset shows the temperature dependent average cell volumes V under selected hydrostatic pressures.

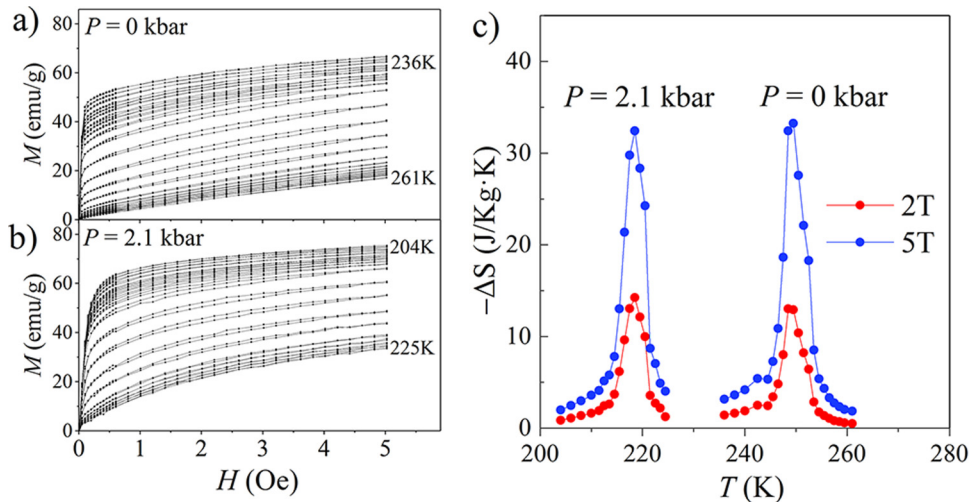


FIG. 6. Isothermal magnetization (M - H) curves of $\text{MnNi}_{0.47}\text{Fe}_{0.53}\text{Si}_{0.46}\text{Ge}_{0.54}$ under (a) ambient pressure and (b) 2.1 kbar. (c) Temperature dependence of magnetic entropy change under 0 kbar and 2.1 kbar for the field changes of 0–2 T and 0–5 T.

increasing pressure. The ΔS_{Latt} under different pressures can be calculated based on the Debye approximation as follows:

$$S_{\text{L}} = -3Nk_{\text{B}} \ln \left[1 - \exp \left(-\frac{\Theta}{T} \right) \right] + 12Nk_{\text{B}} \left(\frac{T}{\Theta} \right)^3 \int_0^{\Theta/T} \frac{x^3}{e^x - 1} dx, \quad (1)$$

where N is the number of atoms per mole and k_{B} is the Boltzmann constant, Θ is the Debye temperature. For the present $\text{MnNi}_{0.47}\text{Fe}_{0.53}\text{Si}_{0.46}\text{Ge}_{0.54}$, the Θ during the transition can be obtained by $\Theta = \Theta_0(1 - \gamma\omega)$, where Θ_0 is the Debye temperature without lattice change and here $\Theta_0 \sim 319$ K according to Ref. 23. γ is the Gruneisen constant, which is calculated from the volume expansion coefficient in the low temperature region based on the Gruneisen law. ω is the maximal volume change during the MST, and here we use the $\Delta V/V$ values refined from the NPD patterns. Accordingly, the ΔS_{Latt} under different pressures can be obtained, which is also plotted in Fig. 5(b) along with the corresponding $\Delta V/V$. It can be seen that the ΔS_{Latt} reduces by $\sim 10\%$ from $37.1 \text{ J kg}^{-1} \text{ K}^{-1}$ to $33.5 \text{ J kg}^{-1} \text{ K}^{-1}$ with pressure increasing from 0 kbar to 2 kbar.

Further, the entropy change ΔS driven by the magnetic field is calculated by using the Maxwell relationship $\Delta S = \int_0^H \left(\frac{\partial M}{\partial T} \right)_{P,H} dH$ based on series of isothermal magnetization (M - H curves). Figures 6(a) and 6(b) show the M - H curves of the $\text{MnNi}_{0.47}\text{Fe}_{0.53}\text{Si}_{0.46}\text{Ge}_{0.54}$ compound under pressures 0 kbar and 2.1 kbar, respectively. It can be seen that there is a small hysteresis between the rising and falling branches around the MST, while the hysteresis area remains nearly unchanged with the application of pressure. The calculated ΔS at different pressures and magnetic fields (0–2 T and 0–5 T) are shown in Fig. 6(c). For a field change of 0–5 T, the $-\Delta S$ peaks around ~ 250 K with maximum value $\sim 33.3 \text{ J kg}^{-1} \text{ K}^{-1}$ under 0 pressure. An application of 2.1 kbar

pressure shifts the $-\Delta S$ peak to ~ 219 K with a nearly unchanged corresponding peak value $32.4 \text{ J kg}^{-1} \text{ K}^{-1}$ at 5 T. These entropy changes ΔS driven by a 5 T magnetic field under both 0 and 2.1 kbar are somewhat smaller compared to the lattice entropy change ΔS_{Latt} driven by the temperature across the MST [Fig. 5(b)]. This result may reflect that the MST driven by a magnetic field up to 5 T cannot be completed, which is consistent with the measured M - T curves shown in the inset of Fig. 3.

IV. CONCLUSION

In summary, $\text{MnNi}_{1-x}\text{Fe}_x\text{Si}_{1-y}\text{Ge}_y$ alloys were prepared, and the magnetostructural transition (MST) was realized in a few compositions through adjusting Fe- and Ge-doping. $\text{MnNi}_{0.47}\text{Fe}_{0.53}\text{Si}_{0.46}\text{Ge}_{0.54}$ was chosen to perform NPD studies on hydrostatic pressure regulated MST and MCE. Careful refinements revealed that the martensitic orthorhombic phase shows a linear FM structure with the magnetic moment confined on Mn sites and the direction along the b axis. A ≤ 5 kbar pressure can slightly compress the lattice, but the induced change of Mn–Mn bond lengths is not enough to affect the spin structure and magnetic moment on Mn atoms. The MST keeps sharp under a small pressure but notably slows down as the pressure reaches 5 kbar, and this may be ascribed to the extended temperature region of the coexistent FM orthorhombic and the non-magnetic hexagonal phase, instead of the decoupling of MST. From the NPD results, the derived $\Delta V/V$ across MST reduces 7% as a pressure 2.1 kbar is applied, and the estimated lattice entropy change (ΔS_{Latt}) reduces by 10% based on the Debye approximation accordingly. These ΔS_{Latt} values, driven by temperature, are all somewhat larger than the entropy change (ΔS_{Mag}) driven by a 5 T magnetic field, which may imply that a magnetic field of 5 T is not adequate to prompt the MST completed. Our work discloses the mechanism of the pressure regulated MST and MCE from the atomic level for the $\text{MnNi}_{1-x}\text{Fe}_x\text{Si}_{1-y}\text{Ge}_y$ alloys. The results are helpful for understanding the regulated MCE by multiple fields for the materials with MST.

ACKNOWLEDGMENTS

This work was supported by the National Key Research and Development Program of China (Grant Nos. 2017YFB0702702, 2019YFA0704904, 2018YFA0305704, 2017YFA0206300, 2017YFA0303601, and 2016YFB0700903), the National Natural Science Foundation of China (Grant Nos. U1832219, 51531008, 51771223, 51590880, 51971240, 11674378, 11934016, 11921004), and the Key Program and Strategic Priority Research Program (B) of the Chinese Academy of Sciences.

REFERENCES

- ¹V. K. Pecharsky and K. A. Gschneidner Jr., *J. Magn. Magn. Mater.* **200**, 44–56 (1999).
- ²A. M. Tishin and Y. I. Spichkin, *The Magnetocaloric Effect and Its Applications* (Institute of Physics Publishing, Bristol, 2003).
- ³V. K. Pecharsky and K. A. Gschneidner, *Phys. Rev. Lett.* **78**, 4494 (1997).
- ⁴O. Tegus, E. Bruck, K. H. J. Buschow, and F. R. De Boer, *Nature* **415**, 150–152 (2002).
- ⁵H. Wada and Y. Tanabe, *Appl. Phys. Lett.* **79**, 3302–3304 (2001).
- ⁶S. Gama, A. A. Coelho, A. de Campos, A. M. Carvalho, F. C. G. Gandra, P. J. von Ranke, and N. A. de Oliveira, *Phys. Rev. Lett.* **93**, 237202 (2004).
- ⁷F. X. Hu, B. G. Shen, J. R. Sun, Z. H. Cheng, G. H. Rao, and X. X. Zhang, *Appl. Phys. Lett.* **78**, 3675–3677 (2001).
- ⁸B. G. Shen, J. R. Sun, F. X. Hu, H. W. Zhang, and Z. H. Cheng, *Adv. Mater.* **21**, 4545–4564 (2009).
- ⁹A. Fujita, S. Fujieda, Y. Hasegawa, and K. Fukamichi, *Phys. Rev. B* **67**, 104416 (2003).
- ¹⁰F. X. Hu, B. G. Shen, and J. R. Sun, *Appl. Phys. Lett.* **76**, 3460–3462 (2000).
- ¹¹T. Krenke, E. Duman, M. Acet, E. F. Wassermann, X. Moya, L. Manosa, and A. Planes, *Nat. Mater.* **4**, 450–454 (2005).
- ¹²J. Liu, T. Gottschall, K. P. Skokov, J. D. Moore, and O. Gutfleisch, *Nat. Mater.* **11**, 620–626 (2012).
- ¹³E. K. Liu, W. H. Wang, L. Feng, W. Zhu, G. J. Li, J. L. Chen, H. W. Zhang, G. H. Wu, C. B. Jiang, H. B. Xu, and D. B. Frank, *Nat. Commun.* **3**, 873 (2012).
- ¹⁴R. R. Wu, L. F. Bao, F. X. Hu, H. Wu, Q. Z. Huang, J. Wang, X. L. Dong, G. N. Li, J. R. Sun, F. R. Shen, T. Y. Zhao, X. Q. Zheng, L. C. Wang, Y. Liu, W. L. Zuo, Y. Y. Zhao, M. Zhang, X. C. Wang, C. Q. Jin, G. H. Rao, X. F. Han, and B. G. Shen, *Sci. Rep.* **5**, 18027 (2015).
- ¹⁵Y. Y. Zhao, F. X. Hu, L. F. Bao, J. Wang, H. Wu, Q. Z. Huang, R. R. Wu, Y. Liu, F. R. Shen, H. Kuang, M. Zhang, X. Q. Zheng, J. R. Sun, and B. G. Shen, *J. Am. Chem. Soc.* **137**, 1746–1749 (2015).
- ¹⁶F. R. Shen, H. B. Zhou, F. X. Hu, J. T. Wang, S. H. Deng, B. T. Wang, H. Wu, Q. Z. Huang, J. Wang, J. Chen, L. H. He, J. Z. Hao, Z. B. Yu, F. X. Liang, T. J. Liang, J. R. Sun, and B. G. Shen, *Mater. Horiz.* **7**, 804–810 (2020).
- ¹⁷V. Johnson, *Inorg. Chem.* **14**, 1117–1120 (1975).
- ¹⁸W. Bazela, A. Szytula, J. Todorovic, and A. Zieba, *Phys. Stat. Sol. (a)* **64**, 367–378 (1981).
- ¹⁹Z. Gercsi and K. G. Sandeman, *Phys. Rev. B* **81**, 224426 (2010).
- ²⁰Z. Gercsi, K. Hono, and K. G. Sandeman, *Phys. Rev. B* **83**, 174403 (2011).
- ²¹T. Samanta, D. L. Lepkowski, A. U. Saleheen, A. Shankar, J. Prestigiacomo, I. Dubenko, A. Quetz, I. W. H. Oswald, G. T. McCandless, J. Y. Chan, P. W. Adams, D. P. Young, N. Ali, and S. Stadler, *Phys. Rev. B* **91**, 020401 (2015).
- ²²L. Caron, N. T. Trung, and E. Bruck, *Phys. Rev. B* **84**, 020414 (2011).
- ²³J. L. Wang, P. Shamba, W. D. Hutchison, Q. F. Gu, M. F. M. Din, Q. Y. Ren, Z. X. Cheng, S. J. Kennedy, S. J. Campbell, and S. X. Dou, *J. Appl. Phys.* **117**, 17D103 (2015).